Significant contribution of organics to aerosol liquid water content in winter in Beijing, China

Xiaoai Jin[1], Yuying Wang[1,2], Zhanqing Li[3], Fang Zhang[1], Weiqi Xu[4,5], Yele Sun[4,5], Xinxin Fan[1], Guangyu Chen[6], Hao Wu[1], Jingye Ren[1], Qiuyan Wang[2], and Maureen Cribb[3]

[1]State Key Laboratory of Earth Surface Processes and Resource Ecology, College of Global Change and Earth System Science, Beijing Normal University, Beijing 100875, China

[2]Key Laboratory for Aerosol-Cloud-Precipitation of China Meteorological Administration, School of Atmospheric Physics, Nanjing University of Information Science and Technology, Nanjing 210044, China

[3]Department of Atmospheric and Oceanic Science, and Earth System Science Interdisciplinary Center, University of Maryland, College Park, MD, USA

[4]State Key Laboratory of Atmospheric Boundary Layer Physics and Atmospheric Chemistry, Institute of Atmospheric Physics, Chinese Academy of Sciences, Beijing 100029, China

[5]College of Earth Sciences, University of Chinese Academy of Sciences, Beijing 100049, China

[6]Zhejiang Windey Co., Ltd.，Hangzhou 310012，China

Correspondence to: Zhanqing Li (zli@atmos.umd.edu), Yuying Wang (wyy_bnu@126.com)

Abstract

The aerosol liquid water content (ALWC), an important component of atmospheric particles, has a significant effect on atmospheric optical properties, visibility and multiphase chemical reactions. In this study, ALWC is determined from aerosol hygroscopic growth factor and particle number size distribution (PNSD) measurements and also simulated by the ISORROPIA II thermodynamic model with measured aerosol chemical composition data at an urban site in Beijing from 8 November to 15 December 2017. Rich measurements made during the experiment concerning virtually all aerosol properties allow us not only to derive the ALWC but also to study the contributions by various species for which little has been done in this region. The simulated ALWC including the contribution of organics and the calculated ALWC are highly correlated (coefficient of determination R^2 = 0.92). The ALWC contributed by organics ($ALWC_{Org}$) accounts for 30 % ± 22 % of the total ALWC during the sampling period. These results suggest a significant contribution of organics to ALWC, which is rather different from previous studies that showed negligible contributions by organics. Our results also show that ALWC correlates well with the mass concentrations of sulfate, nitrate, and secondary organic aerosols (SOA) (R^2 = 0.66, 0.56, and 0.60, respectively). We further noted that accumulation mode particles play a key role in determining ALWC, dominating among all the aerosol modes. ALWC is an exponential function of ambient relative humidity (RH) whose strong diurnal variation influence the diurnal variation of ALWC. However, there is a three-hour lag between the extremes of ALWC and RH values, due to the diurnal variations in PNSD and aerosol chemical composition. Finally, a case study reveals that $ALWC_{Org}$ plays an important role in the formation of secondary aerosols through multiphase reactions at the initial stage of a heavy haze episode.

1. Introduction

China has experienced rapid economic developments during the past few decades, resulting in frequent heavy haze events. Severe air pollution may harm human health and affect the regional climate through aerosol direct and indirect radiation effects (Li et al., 2016; G. X. Wu et al., 2016). However, air pollution formation mechanisms and aerosol climate effects remain highly uncertain due to the complex physical and chemical processes involved (Tao et al., 2012; Y. Wang et al., 2014).

Aerosol liquid water (ALW), a component of atmospheric particles in the atmosphere, exists universally and plays an important role in many atmospheric physical and chemical processes (Nguyen et al., 2016). For example, ALW can influences aerosol optical properties, resulting in increased extinction coefficients, lowered atmospheric visibilities, enhanced aerosol optical depths (AODs), and changes in the direct climatic effect of aerosols (Dougle et al., 1996; Adams et al., 2001; Liao et al., 2005; Seinfeld and Pandis, 2006). Secondary aerosols (SA) are considered to be the main source of particulate pollution during heavy haze events in China (Huang et al., 2014). Many studies now highlight the significance of aerosol liquid water content (ALWC) in the formation of SA through chemical reactions (e.g., Arellanes et al., 2006; G. Wang et al., 2016; Cheng et al., 2016). This is because ALW can dilute the absolute concentration of solutes, adjust aerosol acidity, and serve as a reactant, resulting in increases in trace gas (e.g., N_2O_5 and HO_2) uptake coefficients (Wahner et al., 1998; Bertram et al., 2009; Abbatt et al., 2012). H. Wang et al. (2017) found that the uptake coefficient of N_2O_5 can be high, which is related to high ALWC in Beijing, thereby increasing the formation of nitrates. ALW can also speed up the aqueous phase chemical reaction by serving as a reactor for the transformation of SO_2 to sulfate (Zheng et al., 2015; G. Wang et al., 2016; Cheng et al., 2016). Some studies have found that ALWC can facilitate the formation of secondary organic aerosols (SOA) through aqueous-phase chemistry and photochemistry (Blando et al., 2001; Surratt et al., 2007; Hennigan et al., 2008; Song et al., 2019). Furthermore, observations in Beijing have shown that aqueous-phase processes play a dominant role in the additional formation of oxidized SOA (Xu et al.,

2017). Overall, investigating the formation of SA and haze in North China requires an examination of ALWC and its factors including aerosol particle number size distribution (PNSD), aerosol chemical composition and ambient related humidity (RH) in this region.

However, directly measuring real-time ALWC is not feasible yet because of technical limitations, (Kuang et al., 2018). Four indirect methods have been proposed to calculate real-time ALWC: (1) the aerosol PNSD under dry conditions and ambient RH conditions are first measured, then ALWC is calculated as the difference between dry and ambient aerosol volumes (Stanier et al., 2004); (2) the increased aerosol volume due to water uptake (i.e., ALWC) is calculated according to the measured dry PNSD, size-dependent aerosol hygroscopicity, and ambient RH (Kitamori et al., 2009; Bian et al., 2014; Tan et al., 2017); (3) the dry and ambient aerosol volumes are first estimated using the measured aerosol optical enhancement and Ångström exponent, then ALWC is calculated as the difference between dry and ambient aerosol volumes (Kuang et al., 2018); and (4) ALWC is simulated using thermal equilibrium models such as the ISORROPIA thermodynamic model (Nenes et al., 1998), Aerosol Inorganics Model models (Wexler and Clegg, 2002), the Simulating Composition of Atmospheric Particles in Equilibrium model (Kim et al., 1993), and the Gibb's Free Energy Minimization model (Ansari et al., 1999) with aerosol chemical composition information as input.

ALWC mostly depends on aerosol PNSD, chemical composition, and ambient RH. Hodas et al. (2014) reported that ALWC in the Po Valley in Italy was driven by locally formed anthropogenic nitrates. The implications for the lifetimes of water-soluble organic compounds and its potential influence on SOA formation were also discussed. Another study also revealed that ALWC in Beijing was driven by secondary inorganic aerosols (SIA; Z. Wu et al., 2018). Most previous studies have focused on the interaction between inorganic salts and ALWC, but the impact of organic species on ALWC been ignored to our knowledge (Blando et al., 2001; Surratt et al., 2007; Hennigan et al., 2008; Carlton et al., 2014). A thorough understanding of the association of ALWC with organic aerosols in the atmosphere is lacking.

In this study, ALWC is calculated using the indirect method (2) and simulated using the ISORROPIA II model, i.e., indirect method (4), discussed previously. The effects of inorganic aerosols, organic aerosols, PNSD, and ambient RH on ALWC are then investigated separately. We demonstrate the significant contribution of organics to ALWC in Beijing and provide evidence that the ALW contributed by organics serves as a reactor for sulfate and SOA formation.

2. Data and measurements

2.1. Sampling site

The Air Pollution and Human Health (APHH) winter field campaign took place from 8 November to 15 December 2016 at the Chinese Academy of Sciences' Institute of Atmospheric Physics Tower Branch in Beijing. Beijing is located in the northwest part of the North China Plain, which has experienced rapid economic developments during the last few decades. A large amount of gaseous precursors and other air pollutants are emitted in this region every year, causing serious air pollution problems. The sampling site is located in the northwestern urban area of Beijing (39.97°N, 116.37°E), between the north third and fourth ring roads and surrounded by restaurants. Traffic and cooking emissions are thus the main pollutants at the site. Aerosols at this site can, therefore, well represent anthropogenic aerosols in highly polluted areas. Sun et al. (2013) and Y. Wang et al. (2017) provide more detailed descriptions of the sampling site.

2.2. Instrumentation

Sampling instruments used during the field campaign included a scanning mobility particle sizer (SMPS) equipped with a long differential mobility analyzer (DMA; model 3081A, TSI) and a condensation particle counter (CPC; model 3772, TSI). A custom-built hygroscopicity tandem differential mobility analyzer (H-TDMA) was installed in an air-conditioned mobile container at ground level. The temperature inside the container was maintained at 20–25^{o}C. A high-resolution

aerosol mass spectrometer (HR-AMS) was set up in a sampling room located on a two-story roof, about 25 m north from the container. Sampled air went through a $PM_{2.5}$ cyclone inlet fixed on the top of the container before entering the instruments. The RH of the sampled air was dried to below 20 % by a dryer system consisting of a tube filled with silica gel and a Nafion dryer (model PD-70T-24ss, Perma Pure Inc., USA). Various meteorological parameters, including wind speed (WS), wind direction (WD), temperature (*T*), and RH, were measured from a 325-m meteorological tower located ~20 m west of the container. In this study, all times are reported in Beijing local time (UTC+8 h).

PNSDs with electrical-mobility diameters ranging from 10 to 600 nm were measured by a scanning mobility particle sizer (SMPS) at a 5-min time resolution. PNSDs were extended to diameters ranging from 0.6 to 1 μm by fitting the measured PNSDs with functions consisting of three-mode log-normal distributions (Hussein et al., 2005). Thus generated are PNSDs with a diameter range of 10 nm to 1 μm.

The H-TDMA system developed by the Guangzhou Institute of Tropical and Marine Meteorology measured the size-dependent aerosol hygroscopic growth factor (GF). The H-TDMA system mainly consists of four parts. The first part is a Nafion dryer to keep the RH of sampled air below 20 % and a bipolar neutralizer (soft X-ray, model 3088, TSI Inc.) to equilibrate the particle charge (Wiedensohler et al., 1988). Next, the sampled air passes through the first differential mobility analyzer (DMA1; model 3081L, TSI Inc.) to produce mono-dispersed particles. In this study, the diameters were set to 40, 80, 110, 150, and 200 nm. The sampled air then went through a Nafion humidifier (model PD-70T-24ss, Perma Pure Inc., USA) used to humidify the RH of sampled air to 90 %. The last part of the H-TDMA is the second DMA (same model as the DMA1) and a water-based condensation particle counter (model 3787, TSI Inc.), used to measure the number size distribution of humidified particles in the five selected diameters. Y. Wang et al. (2017) provide a detailed introduction to the H-TDMA system.

Size-resolved non-refractory sub-micron aerosol chemical species, including organics (Org),

sulfate (SO_4^{2-}), nitrate (NO_3^-), ammonium (NH_4^+), and chloride (Cl^-), were measured by the HR-AMS. The sampled air dried by diffusion silica gel dryers was drawn into the HR-AMS through a $PM_{2.5}$ cyclone inlet to remove coarse particles larger than 2.5 μm. The HR-AMS was calibrated with pure ammonium nitrate following the procedures detailed in Jimenez et al. (2003). Sun et al. (2016b) provide operational details about the HR-AMS.

3. Method

3.1. ALWC calculation based on H-TDMA measurements

The ALWC is calculated based on measurements of the aerosol GF and particle number size distribution. Briefly, H-TDMA data are first used to derive the size-resolved particle GFs at various RHs. Then ALWC is calculated as the increased aerosol volume due to hygroscopic growth attributed to water uptake.

Chen et al. (2012) showed how to calculate size-resolved particle GFs at different RHs. First, a three-mode log-normal distribution is applied to fit the measured PNSD to produce fitting parameters for each mode. The hygroscopicity parameter (κ) in any mode is assumed to be constant. The H-TDMA-derived size-dependent κ can then be used to deduce the corresponding κ for the nucleation mode, the Aitken mode, and the accumulation mode of PNSDs according to the following equation:

$$\kappa(D_P) = \frac{\sum_{i=1}^{3} \kappa_i \cdot N_i(D_p)}{\sum_{i=1}^{3} N_i(D_p)}, \quad (1)$$

where κ_i refers to the κ of the ith mode, and N_i (D_p) refers to the number concentration of particles in the ith mode. According to κ-Köhler theory (Petters and Kreidenweis, 2007), κ at a certain diameter (D_d) can be calculated as

$$\kappa(D_d) = (GF^3 - 1) \cdot \left[\frac{1}{RH} \exp\left(\frac{4\sigma_{s/a} M_w}{RT\rho_w D_d GF}\right) - 1\right], \quad (2)$$

where RH is the control value by the humidifier in the H-TDMA system, T is the mean room temperature of the container set to 293 K, $\sigma_{s/a}$ is the surface tension of the solution/air interface assumed

to be the same as the surface tension coefficient between water and air (about 0.0728 N m^{-1} at 293 K), M_w is the molecular weight of water, R is the universal gas constant, ρ_w is the density of water, and D_d is the diameter of the dry particles. The GF at a given RH is defined as the ratio of the humidified diameter [D_p (RH)] to D_d:

$$\mathrm{GF} = D_p(\mathrm{RH})/D_d \ . \quad (3)$$

The known κ of each mode derives the size-resolved κ at 90 % RH using Eq. (1). Substituting the size-resolved κ into Eq. (2) results in size-resolved GFs at various RHs. Finally, the volume of ALWC at ambient RH is equal to the increased aerosol volume due to water uptake, i.e., ALWC can be calculated as

$$\mathrm{ALWC_{HTDMA}} = \left[\frac{1}{6}\sum_i n_i D_{p,i}^3 \left(GF\left(D_{p,i}, RH\right)^3 - 1\right)\right] \cdot \rho_w \ , \quad (4)$$

where n_i refers to the particle number concentration of dry particles for the corresponding particle size range in the ith mode, and $D_{p,i}$ refers to the particle diameter for the corresponding particle size range.

3.2. ALWC simulations based on the ISORROPIA II model

The thermodynamic equilibrium model ISORROPIA II developed by Fountoukis and Nenes (2007) using aerosol chemical composition information from the HR-AMS can simulate ALWC ($ALWC_{ISO}$). The bulk chemical composition was used in the model. However, the ISORROPIA II model only considers the contribution of inorganic species (Ca^{2+}, K^+, Mg^{2+}, NH^+, Na^+, SO_4^{2-}, NO_3^-, Cl^- and H_2O) on ALWC and neglects the contribution of organics. In this study, the phase state was assumed to be stable in the model calculation, and the model was set up to reverse mode due to the lack of measurements of gaseous ammonia.

According to the model assumptions that the aerosol curvature effect in Köhler theory is ignored, and the aerosol water uptake has no effect on ambient vapor pressure, the water activity (a_w) defined as the effective mole fraction of water is equal to the ambient RH in this model (Seinfeld and Pandis, 2006):

$$a_w = RH \quad (5)$$

The ALWC can be calculated using the Zdanovskii−Stokes−Robinson (ZSR) mixing rule (Stokes and Robinson, 1966),

$$\mathrm{ALWC_{ISO}} = \sum_i \frac{M_i}{m_{0i}(a_w)}, \quad (6)$$

where M_i is the mole concentration of the ith species (mol m^{-3} in air), and m_{0i} (a_w) is the corresponding molality of the binary solution of the ith species under the same a_w with complex solution. Finally, with measured ambient RH and T values as input $\mathrm{ALWC_{ISO}}$ values under different RH and T conditions can be derived.

3.3. Inferring the contribution of organics to ALWC

According to the κ-Köhler theory and the ZSR mixing rule, κ can also be expressed as the sum of the contributions of each aerosol component:

$$\kappa = \sum_i \varepsilon_i \kappa_i, \quad (7)$$

where ε_i and κ_i are the volume fraction and hygroscopicity of the ith species, respectively. Submicron aerosols mainly consist of organic and inorganic species (Carbone et al., 2013; Zieger et al., 2017). As mentioned in section 2.2, the HR-AMS measures the mass concentrations of organics and inorganics, including SO_4^{2-}, NO_3^-, NH_4^+, and Cl^-. The volume fraction of inorganic species can be calculated based on the ion-pairing scheme given by the following equations (Gysel et al., 2007):

$$n_{\mathrm{NH_4NO_3}} = n_{\mathrm{NO_3^-}},$$

$$n_{\mathrm{NH_4HSO_4}} = \min\left(2n_{\mathrm{SO_4^{2-}}} - n_{\mathrm{NH_4^+}} + n_{\mathrm{NO_3^-}}, n_{\mathrm{NH_4^+}} - n_{\mathrm{NO_3^-}}\right),$$

$$n_{\mathrm{(NH_4)_2SO_4}} = \max\left(n_{\mathrm{NH_4^+}} - n_{\mathrm{NO_3^-}} - n_{\mathrm{SO_4^{2-}}}, 0\right),$$

$$n_{H_2SO_4} = \max\left(0, n_{\mathrm{SO_4^{2-}}} - n_{\mathrm{NH_4^+}} + n_{\mathrm{NO_3^-}}\right),$$

$$n_{\mathrm{HNO_3}} = 0, \quad (8)$$

where n represents the mole numbers, and "min" and "max" are minimum and maximum values,

respectively. The κ values of the inorganic species sulfuric acid, ammonium sulfate, ammonium hydrogen sulfate, and ammonium nitrate are 1.19, 0.48, 0.56, and 0.58, respectively (Topping et al., 2005; Petters and Kreidenweis, 2007). So the ZSR model can be used to estimate the contribution of inorganic species to the κ value. In this paper, the chloride was not taken into account in ion-pairing because its source is hard to determine. This may result in a minor uncertainty in κ calculation. The hygroscopicity parameter of organics (κ_{Org}) can be calculated using the volume fraction of organics and the total κ value derived from the H-TDMA, according to Eq. (7). Finally, the ALWC contributed by organic species ($ALWC_{Org}$) can be calculated as (Petters and Kreidenweis, 2007)

$$ALWC_{Org} = \frac{m_{Org}\rho_W}{\rho_{Org}} \frac{\kappa_{Org}}{\left(\frac{1}{RH}-1\right)}, \quad (9)$$

where m_{Org} is the organic mass concentration from the AMS (Xu et al., 2015), and ρ_{Org} is the density of organics, taken as 1.4 g cm^{-3} (Moore et al., 2011; Lathem et al., 2013; Cerully et al., 2014).

4. Results and discussion

4.1. Comparison of calculated and simulated ALWC

The trends in ALWC calculated based on the hygroscopic growth factor and PNSD ($ALWC_{HTDMA}$) and simulated from ISOPPOPIA II model ($ALWC_{ISO}$) are generally consistent. Figure 1a shows that $ALWC_{HTDMA}$ and $ALWC_{ISO}$ agree well and that their coefficient of determination (R^2) is 0.89. The correlation is especially strong for RH over 90 %. However, for RH below 60 %, $ALWC_{ISO}$ is less than $ALWC_{HTDMA}$ and even close to 0 in some cases. Bian et al. (2014) and Tan et al. (2017) observed a similar phenomenon in northern and southern China. There are three possible explanations for these results. H-TDMA samples were humidified to 90 % RH during the field campaign, thereby leading to the neglect of the deliquescence process in the $ALWC_{HTDMA}$ calculation. This may lead to overestimation of $ALWC_{HTDMA}$ for RH below the deliquescence relative humidity (DRH). Second, the assumption of constant κ in each mode may lead to small uncertainty in size-resolved GFs at different RHs, resulting in small deviation in ALWC calculation. This may be another reason for the difference

between $ALWC_{HTDMA}$ and $ALWC_{ISO}$. In addition, the ISORROPIA II model ignores the effect of aerosol shape and complex organic species on the DRH. Previous studies have suggested that the particle spherical assumption and simplified aerosol chemical species in this model can overestimate the DRH (Seinfeld and Pandis, 2006; Sjogren et al., 2007). So for RH below the simulated DRH (~60 %), particles may still be dry in the ISORROPIA II model, but may have been hydrated in the real atmosphere. Therefore, this model underestimates ALWC. The ambient aerosol deliquescent phenomenon is rare in the North China Plain (Kuang et al., 2016). In addition, the ISORROPIA II model cannot simulate water uptake by organics, which can lead to some bias between simulated and calculated ALWCs. As described in section 3.3, $ALWC_{Org}$ can be inferred and used to discuss differences between $ALWC_{ISO}$ and $ALWC_{HTDMA}$. Figure 1b shows that adding $ALWC_{Org}$ to $ALWC_{ISO}$ leads to a stronger correlation with $ALWC_{HTDMA}$ (R^2 = 0.92). The correlation improves significantly for RH below 60 %. This demonstrates that (1) organic species contribute significantly to ALWC, and (2) the underestimation of ALWC by the ISORROPIA II model is also related to the neglect of organic species in the model.

4.2. Impact of different factors on ALWC

4.2.1. Impact of aerosol chemical species on ALWC

Figure 2 shows the characteristics of seven heavy pollution events selected for examination. Figures 2a and 2c display the time series of WS, WD, and ambient RH. The prevailing wind during the haze episodes was a weak southerly wind that was favorable for bringing in pollutants from the highly populated and industrialized neighboring regions to the sampling site. This is beneficial to the formation and accumulation of SA (T. Wang et al., 2010; Y. Wang et al., 2017). However, the prevailing winds during the clean events were strong northerly winds that always carried in a clean air mass, resulting in pollutants being quickly removed (Figure 2c). Note that the PM_1 mass concentration

decreases somewhat in the evening during haze episodes, following the short-term change of WD from southerly to northerly. This is related to mountain-valley breezes in Beijing (Wehner et al., 2008; Gao et al., 2011; Y. Wang et al., 2017). These results demonstrate that heavy haze episodes have a strong correlation with local wind direction in Beijing.

Figures 2a and 2d show the time series of ambient RH and mass concentrations of aerosol chemical species in PM_1. These figures suggest that the increase in inorganic and organic aerosols is synchronous with the increase in ambient RH during the heavy pollution periods (P1-P7). This is likely because of a positive feedback mechanism driven by Henry's law and thermodynamic equilibrium (Z. Wu et al., 2018). Figure 2b also shows that ALWC continuously increases during the pollution accumulation period. On average, ALWC increases from 8 to 89 μg m^{-3} as ambient RH increases from 15 to 80 %, and the inorganic and organic aerosol mass concentrations increase from 15 to 120 μg m^{-3} and from 12 to 78 μg m^{-3}, respectively. These results imply that the increase in ambient RH and aerosol mass concentration are all important for the increase in ALWC.

Equation (4) also suggests that the absolute value of ALWC is dependent on the value of ambient RH and aerosol chemical composition (i.e., the GF value). To further investigate the impact of chemical composition on ALWC, the impact of RH on ALWC should be accounted for. Previous studies suggest there is an exponential relationship between ALWC and RH (e.g., Z. Wu et al., 2018). Here, we define the relative ALWC as the ratio of $ALWC_{HTDMA}$ and the function of ambient RH (e^{bRH}). The b is derived according to the relationship between $ALWC_{HTDMA}$ and RH that is fitted by the function $y = ae^{bx}$. Figure 3a shows the relationship between relative ALWC and primary aerosols (PA) or SA mass concentrations. PA consists of primary organic aerosols (POA) and black carbon (BC), and SA consists of SOA, sulfate, and nitrate. The positive matrix factorization (Paatero and Tapper, 1994) was applied on the organic aerosols (OA) spectral matrices to identify POA and SOA. The relative ALWC is highly correlated with SA mass concentrations (R^2 = 0.94) but poorly correlated with PA mass concentrations (R^2 = 0.69). High relative ALWCs coincident with high SA mass

concentrations suggest that SA plays a key role in the increase in ALWC. This is likely because SA is mainly generated from photochemical reactions in the daytime or reactions at night, making SA highly aged with a hygroscopicity stronger than that of PA (Ervens et al., 2011; Sareen et al., 2017). SA can, therefore, absorb more water vapor than PA in the atmosphere. The enhanced aerosol liquid water induced by SA is further favorable for the formation of SA by speeding up the atmospheric chemical reaction rate and serving as the medium for gas-particle heterogeneous reactions (G. Wang et al., 2016; Cheng et al., 2016). This further increases the bulk aerosol hygroscopicity. This is also the reason why inferred κ based on the ZSR model continuously increases during haze episodes (Figure 2c).

Secondary aerosols are mainly composed of nitrate, sulfate, ammonium and SOA. To determine which species is the driver for ALWC in Beijing, Figure 3b shows the correlation analysis between relative ALWC and the mass concentrations of different aerosol chemical species. Relative ALWC and all SIA agree well [R^2 equal to 0.66 (sulfate) and 0.56 (nitrate)]. It has been reported that ALWC is driven by inorganic salts with both nitrate and sulfate playing key roles in determining ALWC (Z. Wu et al., 2018). ALWC also agrees well with SOA (R^2 = 0.60) in our study. This is unexpected because the hygroscopicity of SOA is relatively lower than that of nitrate and sulfate. Some studies have also suggested that the water uptake of aged organics accounts for only a few percent of the total aerosol water uptake (e.g., Gysel et al., 2007; Engelhart et al., 2011). In our study, the contribution of $ALWC_{Org}$ to total ALWC is significant, accounting for 30 % ± 22 %. As shown in Figure 4, the contribution of organics to total ALWC varies strongly. This is likely related with the variation in mass fraction and hygroscopicity parameter of organics (κ_{org}). The mass concentration of inorganics increases more than that of organics as RH increases, leading to a lower mass fraction of organics in the case of high ambient RH. Figure 4 also shows $ALWC_{Org}$ fraction increases significantly with the increase of κ_{org}. All these help explain a large variation in the $ALWC_{Org}$ contribution to total ALWC. Considering the distinct ambient RH and κ_{org} between clean and polluted periods, we calculated respectively the fraction of $ALWC_{Org}$ during two periods. There is a higher $ALWC_{Org}$ fraction (33% ± 23%) during

clean periods than that during polluted periods (26% ± 11%). Yet, there is little variability of $ALWC_{Org}$ fraction during polluted periods. The larger variability in $ALWC_{Org}$ fraction during clean periods is likely caused by the highly variable κ_{org} when the ambient RH is low. In summary, the contribution of organics in total ALWC varies with the variations of the mass fraction of organics and κ_{org}, and this contribution is significant during both clean and polluted periods. Studies of ALWC in Beijing, therefore, cannot neglect $ALWC_{Org}$. This is different from the studies in other regions such as in the Po Valley in Italy (Hodas et al., 2014) and the eastern U.S. (Carlton et al., 2013) where the ALWC was found to be only driven by nitrate and sulfate respectively.

An interesting phenomenon is frequently observed at the initial stage of heavy haze episodes (e.g., P4, P5, P6, and P7). $ALWC_{ISO}$ is almost close to 0, but both $ALWC_{HTDMA}$ and $ALWC_{Org}$ are always larger than 0, and the organic aerosol mass fraction is high at this stage. These observations reveal that at the initial stage of heavy haze episodes, the ALWC is mostly contributed by organic species. Meanwhile, κ is not very low and increases markedly as the PM_1 mass concentration increases, which is unexpected because of the lower hygroscopicity of organic aerosols compared to SIA. Therefore, some highly hygroscopic substance (i.e., SA) must be generated through multiphase chemical reaction at this stage. We propose that the liquid water contributed by organic species provides a reactor for the transformation of gaseous precursors to SA at the initial stages of heavy haze episodes, increasing the uptake of more liquid water by more SA and further accelerating the formation of heavy haze. Section 4.3 provides a case study to demonstrate this.

4.2.2. Impact of PNSD on ALWC

In addition to aerosol chemical composition, ALWC also depends on PNSD (Bian et al., 2014). As described in section 3.1, the nucleation mode (< 30 nm), the Aitken mode (30–110 nm), and the accumulation mode (110 nm to1 μm) (Whitby, 1978; Birmili et al., 2001) are considered in this study. Particles with diameters greater than 1 μm are not considered because some particles in the coarse mode are water soluble but their contribution on the ALWC is low (e.g., Hussein et al., 2004; S. Liu et

al., 2008; Bian et al., 2014; Tan et al., 2017).

Figure 5 in the supplement shows that the contributions of nucleation mode, Aitken mode, and accumulation mode particles to ALWC are < 1.0 %, 18.0 %, and 82.0 %, respectively. Figure 6 shows the correlations between $ALWC_{HTDMA}$ and the volume concentrations of different mode particles, and the average contribution of different mode particles to $ALWC_{HTDMA}$ (f_{ALWC}) under five different RH conditions. The R^2 and f_{ALWC} of the nucleation mode particles (left column in Figure 6) are all less than 0.1 and 1 %, respectively, under all RH conditions. This is likely because the volume concentration of nucleation mode particles is very low, and most of these small particles are composed of hydrophobic chemical species such as BC and POA. Similarly, the number concentration of Aitken mode particles also shows weak correlations with $ALWC_{HTDMA}$ ($R^2 < 0.2$) under RH < 90 % conditions, but their correlation ($R^2 = 0.25$) is enhanced significantly under RH > 90 % conditions (middle column of Figure 6). This is because there are more aged particles in the Aitken mode which can absorb much more water when the ambient RH is higher than 90 %. However, the contribution of the Aitken mode to ALWC ranges from 14 % to 21 % and decreases as RH increases. $ALWC_{HTDMA}$ is strongly correlated to the volume concentration of accumulation mode particles, with R^2 and f_{ALWC} greater than 0.6 and 75 %, respectively, under all RH conditions (right column of Figure 6). Figure 6 also shows that ALWC increases slightly as the volume concentration of accumulation mode particles increases under RH < 70 % conditions (slope < 0.001), but increases strongly under higher RH conditions, especially under RH > 90 % conditions (slope = 0.0041). This is likely because there are more accumulation mode SA formed due to multiphase chemical reactions under high ambient RH conditions. Swietlicki et al. (1999) have suggested that the contribution of accumulation mode particles to ALWC is largest for all-mode particles.

In summary, the contribution of nucleation mode particles to ALWC is very low. The contribution of Aitken mode particles is much higher than nucleation mode particles and decreases with increasing ambient RH. The contribution of accumulation mode particles to ALWC is largest under all RH

conditions and increases with increasing ambient RH, thus playing a key role in determining ALWC.

4.2.3. Impact of RH on ALWC

As discussed in 4.2.1, the absolute value of ALWC has an exponential relationship with ambient RH. Figure 7 shows the relationship between ALWC and RH for different PM_1 mass concentration ranges. ALWC increases slowly as RH increases under lower ambient RH conditions then sharply increases when RH exceeds a critical RH value. This critical RH value is different for different PM_1 mass concentrations. This is because the low RH conditions cannot provide enough water for aerosol particles, even though the PNSD is dominated by accumulation mode particles with higher hygroscopicity (Tan et al., 2016). This demonstrates the important influence of RH on ALWC. The lower critical RH value for higher PM_1 mass concentrations (~80 %) suggests that ALWC is easily formed under heavily polluted conditions. This is likely because there are more SA and accumulation mode particles during pollution periods (Sun et al., 2016a; Y. Wang et al., 2017).

Figure 8a shows the diurnal variations of $ALWC_{HTDMA}$ and ambient RH during the sampling period. The extreme $ALWC_{HTDMA}$ values appear at night and during the day respectively, likely related to the diurnal variations of ambient RH. The elevated ambient RH at night not only increases ALWC through water uptake of particles directly, but also facilitates the formation of hydrophilic particulate nitrate through the speeding up of the uptake coefficient of N_2O_5 (Thornton et al., 2003; Bertram et al., 2009). This can further enhance ALWC. However, although the diurnal variations of $ALWC_{HTDMA}$ and ambient RH are similar, the peak and nadir of $ALWC_{HTDMA}$ (0300 LT and 1100 LT, respectively) appear three hours earlier than the peak and nadir of ambient RH (0600 LT and 1400 LT, respectively). This time difference is likely related to changes in PNSD. The diurnal variation of PNSD (Figure 8b) shows that the number concentrations of Aitken and accumulation mode particles begin to decrease quickly at 0300 LT. ALWC also begins to decrease, although the ambient RH increases slightly at that time. In the morning, ALWC decreases sharply following the ambient RH and PNSD changes due to the lifting planetary boundary layer height. ALWC decreases to its minimum value at ~1100 LT then

begins to increase quickly. However, ambient RH still decreases at that time and reaches its minimum value at ~1400 LT. The increase in ALWC is likely associated with changes in aerosol chemical species and PNSD. Figure 8b and 8c show that there are many newly formed Aitken and accumulation mode particles and that the fraction of SA increases at noon, likely because of strong photochemical reactions. Y. Wang et al. (2017, 2018) have suggested that daytime photochemical reactions are efficient enough to enhance aerosol hygroscopicity and change the aerosol mixing state from external to internal in North China through the formation of hydrophilic chemical species. All this suggests that ambient RH is not the only determining factor for ALWC. PNSD and aerosol chemical composition are also important for ALWC.

4.3. A case study of the impact of $ALWC_{Org}$ on SA formation

As discussed in section 4.2.1, a hypothesis is proposed that $ALWC_{Org}$ maybe provide a reactor for the formation of secondary species. To verify this hypothesis, the P4 case shown in Figure2 is selected to further analyze the influence of $ALWC_{Org}$ on the formation of secondary aerosols (Figure 9). Figure 9a shows the time series of $ALWC_{HTDMA}$, $ALWC_{ISO}$, and $ALWC_{Org}$ during this case. On 27 November 2017, $ALWC_{ISO}$ was close to 0 all day long because of the low ambient RH, but both $ALWC_{HTDMA}$ and $ALWC_{Org}$ were always larger than 0, increasing with increasing PM_1 mass concentration (Figure 9a). Figure 9a also shows that the fraction of $ALWC_{Org}$ in $ALWC_{HTDMA}$ was high at the initial stage of this pollution case, but this fraction decreased as haze increased. This case was further divided into three periods (Figure 9b). Organics were the most abundant chemical species during the first period (64 %), which explains the high fraction of $ALWC_{Org}$ in $ALWC_{HTDMA}$ at the initial stage of this haze case. The pie charts in Figure 9b also show that both SOA and SIA (sulfate, nitrate, and ammonium) increases from the first to third periods but POA decreases, likely related to multiphase reactions (i.e., aqueous-phase reactions) due to the enhanced ALWC. Time series of f_{44} and the fraction of sulfate in total sulfur (F_{SO4}^{2-}) are also shown to further illustrate the influence of aqueous-phase reactions on aerosol chemical species. The m/z 44 signal intensity f_{44} (mostly contributed by the CO_2^+ ion) measured by the

AMS can be used as an indicator of the oxidation level in organic species (Mei et al., 2013). The sulfur oxidation ratio F_{SO4}^{2-} (Sun et al., 2006) is defined as

$$F_{SO_4^{2-}} = \frac{n[SO_4^{2-}]}{n[SO_4^{2-}]+n[SO_2]}, \quad (10)$$

where $n[SO_4^{2-}]$ and $n[SO_2]$ refer to the molar concentrations of SO_4^{2-} and SO_2, respectively. Figure 9b suggests that f_{44} and F_{SO4}^{2-} both increase gradually with increasing $ALWC_{HTDMA}$ and PM_1 mass concentration from 27 November to 30 November 2017. This is likely because the increase in ALWC is beneficial to the oxidation of organics and the transformation of SO_2 to SO_4^{2-}, implying the importance of aqueous-phase chemical reaction on haze formation in Beijing. The production of secondary organic and inorganic species can further enhance aerosol hygroscopicity, increasing ALWC in the atmosphere. This positive feedback is the reason behind the rapid formation of heavy haze events in Beijing (G. Wang et al., 2016). A rapid increase in f_{44} and F_{SO4}^{2-} was seen during the first period at night on 27 November (shown by green and red arrows in Fig. 9) when organics contributed the most to ALWC. This suggests that ALWC contributed by organics may have played an important role in the formation of secondary species at the initial stage of the pollution event.

5. Conclusions

In this study, the aerosol liquid water content (ALWC) was calculated using the size-resolved aerosol hygroscopic growth factor and the particle number size distribution (PNSD) measured at a Beijing urban site during the APHH winter campaign (8 November to 15 December 2017). Also done were simulations using the ISORROPIA II model with measured aerosol chemical composition data as input data. During the sampling period, seven heavy haze episodes were selected to investigate the influence of different factors (PNSD, ambient RH, and aerosol chemical composition) on ALWC.

The calculated and simulated ALWC ($ALWC_{HTDMA}$ and $ALWC_{ISO}$) agree well (correlation of

439 determination R^2 equal to 0.89). However, $ALWC_{ISO}$ is much lower than $ALWC_{HTDMA}$ for RH below
440 60 %, even approaching zero many times. This deviation is in part attributed to the neglect of the
441 contribution of organics to ALWC ($ALWC_{Org}$) in the ISORROPIA II model, contradicting with
442 previous studies ignoring this contribution. The aerosol hygroscopicity of organics was also derived
443 in this study for use in calculating $ALWC_{Org}$. The sum of $ALWC_{ISO}$ and $ALWC_{Org}$ has a higher
444 correlation (R^2 = 0.92) with the calculated ALWC (i.e., $ALWC_{HTDMA}$), especially for RH below 60 %.
445 This implies that organic aerosols are also an important contributor to ALWC.

446 PNSD, ambient RH, and aerosol chemical composition are all found to affect ALWC significantly.
447 Nucleation mode and Aitken mode particles have little influence on ALWC. Accumulation mode
448 particles play a key role in determining ALWC and dominate among all aerosol modes. ALWC is
449 highly related to the relative humidity (RH) when RH exceeds a critical RH value that is different for
450 different PM_1 mass concentrations. ALWC varies diurnally with its extreme values appearing at night
451 and during the day respectively. The diurnal variation of ambient RH explains this. However, there is
452 a three-hour difference between when the extreme ALWC and RH values occur, caused by the diurnal
453 variations in PNSD and aerosol chemical composition.

454 On average, $ALWC_{Org}$ accounts for ~30 % ± 22 % of the total aerosol liquid water during the
455 sampling period. This shows the significant contribution of organic species to ALWC. Our results
456 suggest that ALWC is not only driven by inorganic salts but also driven by organics in Beijing. This is
457 different from the results obtained in the Po Valley in Italy (Hodas et al., 2014) and the eastern U.S.
458 (Carlton et al., 2013) where the ALWC is driven by nitrate and sulfate respectively. Finally, one case
459 study was used to study the importance of $ALWC_{Org}$ on multiphase chemical reactions. $ALWC_{Org}$ was
460 found to play an important role in the formation of secondary aerosols by speeding up aqueous-phase
461 reactions at the initial stage of heavy haze. Our study is important for investigating the contribution of
462 organics to ALWC and its importance on haze formation in Beijing.
463

Data availability. Data used in the study are available from the first author upon request (201631490012@mali.bnu.edu.cn).

Author contributions. ZL and YW designed the experiment; YW, XJ, and WX carried it out and analyzed the data; other co-authors participated in science discussions and suggested additional analyses. XJ and YW prepared the paper with contributions from all co-authors.

Competing interests. The authors declare no competing interests.

Acknowledgements. This work was funded by the National Key R&D Program of China (grant no. 2017YFC1501702), the National Natural Science Foundation of China (NSFC) research projects (grant nos. 91544217, 41575132, 41675141, 41705125), the Startup Foundation for Introducing Talent of NUIST and the National Basic Research Program of China "973" (grant no. 2013CB955801). We thank all participants of the field campaign for their tireless work and cooperation.

References

Abbatt, J. P. D., Lee, A. K. Y., Thornton, J. A.: Quantifying Trace Gas Uptake to Tropospheric Aerosol: Recent Advances and Remaining Challenges, Chem. Soc. Rev., 41(19), 6555−6581, https://doi.org/10.1039/c2cs35052a, 2012.

Adams, P. J., and Seinfeld, J. H.: General circulation model assessment of direct radiative forcing by the sulfate-nitrate−ammonium−water inorganic aerosol system, J. Geophys. Res.-Atmos., 106, 1097−1111, https://doi.org/ 10.1029/2000JD900512, 2001.

Ansari, A.S., Pandis, S.N.: Prediction of multicomponent inorganic atmospheric aerosol behavior, Atmos. Environ., 33 (5), 745–757, https://doi.org/10.1016/S1352-2310(98)00221-0, 1999.

Arellanes, C., Paulson, S. E., Fine, P. M., and Sioutas, C.: Exceeding of Henry's Law by Hydrogen Peroxide Associated with Urban Aerosols, Environ. Sci. Technol., 40, 4859–4866, https://doi.org/10.1021/es0513786, 2006.

Bertram, T. H., Thornton, J. A.: Toward a general parameterization of N_2O_5 reactivity on aqueous particles: the competing effects of particle liquid water, nitrate and chloride, Atmos. Chem. Phys., 9 (21), 8351−8363, https://doi.org/10.5194/acp-9-8351-2009, 2009.

Bian, Y.X., Zhao, C.S., Ma, N., Chen, J., Xu, W.Y.: A study of aerosol liquid water content based on hygroscopicity measurements at high relative humidity in the North China Plain, Atmos. Chem. Phys., 14 (12), 6417–6426, https://doi.org/10.5194/acp-14-6417-2014, 2014.

Birmili, W., Wiedensohler, A., Heintzenberg, J., and Lehmann, K.: Atmospheric particle number size distribution in central Europe: Statistical relations to air masses and meteorology, J. Geophys. Res.-Atmos., 106, 32005–32018, https://doi.org/10.1029/2000JD000220, 2001.

Blando, J. D., Turpin, B. J.: Secondary organic aerosol formation in cloud and fog droplets: a literature evaluation of plausibility, Atmos. Environ., 34, 1623−1632, https://doi.org/10.1016/S1352-2310(99)00392-1, 2001.

Carbone, S., Saarikoski, S., Frey, A., Reyes, F., Reyes, P., Castillo, M., Gramsch, E., Oyola, P., Jayne, J., Worsnop, DR., and Hillamo, R.: Chemical characterization of submicron aerosol particles in Santiago de Chile, Aerosol Air Qual. Res., 13(2), 462-473, https://doi.org/10.4209/aaqr.2012.10.0261, 2013.

Carlton, A. G., Turpin, B. J.: Particle partitioning potential of organic compounds is highest in the Eastern US and driven by anthropogenic water, Atmos. Chem. Phys., 13 (20), 10203−10214, https://doi.org/10.5194/acp-13-10203-2013, 2013.

Cerully, K. M., Bougiatioti, A., Hite Jr., J. R., Guo, H., Xu, L., Ng, N. L., Weber, R., and Nenes, A.: On the link between hygroscopicity, volatility, and oxidation state of ambient and water-soluble aerosol in the Southeastern United States, Atmos. Chem. Phys., 14, 30835–30877, https://doi.org/10.5194/acpd-14-30835- 2014, 2014.

Chen, J., Zhao, C. S., Ma, N., Liu, P. F., Göbel, T., Hallbauer, E., Deng, Z. Z., Ran, L., Xu, W. Y., Liang, Z., Liu, H. J., Yan, P., Zhou, X. J., and Wiedensohler, A.: A parameterization of low visibilities for hazy days in the North China Plain, Atmos. Chem. Phys., 12, 4935–4950, https://doi.org/10.5194/acp-12-4935-2012, 2012.

Cheng, Y., Zheng, G., Wei, C., Mu, Q., Zheng, B., Wang, Z., Gao, M., Zhang, Q., He, K., Carmichael, G., Pöschl, U., Su, H.: Reactive nitrogen chemistry in aerosol water as a source of sulfate during haze events in China, Sci. Adv., 2 (12), e1601530, https://doi.org/10.1126/sciadv.1601530, 2016.

Dougle, P. G., Vlasenko, A. L., Veefkind, J. P., and Brink, H. M. T.: Humidity dependence of the light scattering by mixtures of ammonium nitrate, ammonium sulfate and soot, J. Aerosol. Sci., 27, 513–514, https://doi.org/10.1016/0021-8502(96)00329-1, 1996.

525 Engelhart, G.J., Hildebrandt, L., Kostenidou, E., Mihalopoulos, N., Donahue, N.M., Pandis, S.N.:
526 Water content of aged aerosol, Atmos. Chem. Phys., 11, 911–920, https://doi.org/10.5194/acp-11-
527 911-2011, 2011.
528 Ervens, B., Turpin, B. J., Weber, R. J.: Secondary organic aerosol formation in cloud droplets and
529 aqueous particles (aqSOA): a review of laboratory, field and model studies, Atmos. Chem. Phys.,
530 11 (21), 11069−11102, https://doi.org/10.5194/acp-11-11069-2011, 2011.
531 Fountoukis, C. and Nenes, A.: ISORROPIA II: a computationally efficient thermodynamic equilibrium
532 model for K^+– Ca^{2+}–Mg^{2+}–$NH4^+$–Na^+–SONO –Cl^-–H_2O aerosols, Atmos. Chem. Phys., 7, 4639–
533 4659, https://doi.org/10.5194/acp-7-4639-2007, 2007.
534 Gao, Y., Liu, X., Zhao, C., and Zhang, M.: Emission controls versus meteorological conditions in
535 determining aerosol concentra- tions in Beijing during the 2008 Olympic Games, Atmos. Chem.
536 Phys., 11, 12437–12451, https://doi.org/10.5194/acp-11-12437-2011, 2011.
537 Gysel, M., Grosier, J., Topping, D.O., Whitehead, J.D., Bower, J.N., Cubison, M.J., Williams, P.I.,
538 Flynn, M.J., McFiggans, G.B., Coe, H.: Closure study between chemical composition and
539 hygroscopic growth of aerosol particles during TORCH2, Atmos. Chem. Phys., 7 (24), 6131–6144,
540 https://doi.org/10.5194/acp-7-6131-2007, 2007.
541 Hennigan, C. J., Bergin, M. H., Dibb, J. E., Weber, R. J.: Enhanced secondary organic aerosol
542 formation due to water uptake by fine particles, Geophys. Res. Lett., 35(18), No. L18801,
543 https://doi.org/10.1029/2008GL035046, 2008.
544 Hodas, N., Sullivan, A. P., Skog, K., Keutsch, F. N., Collett, J. L., Decesari, S., Facchini, M. C.,
545 Carlton, A. G., Laaksonen, A., Turpin, B. J.: Aerosol Liquid Water Driven by Anthropogenic Nitrate:
546 Implications for Lifetimes of Water-Soluble Organic Gases and Potential for Secondary Organic
547 Aerosol Formation, Environ. Sci. Technol., 48 (19), 11127−11136
548 https://doi.org/10.1021/es5025096, 2014.
549 Huang, R., Zhang, Y., Bozzetti, C., Ho, K., Cao, J., Han, Y., Daellenbach, K. R., Slowik, J. G., Platt,
550 S. M., Canonaco, F.: High secondary aerosol contribution to particulate pollution during haze events
551 in China, Nature., 514 (7521), 218, https://doi.org/10.1038/nature13774, 2014,.
552 Hussein, T., Puustinen, A., Aalto, P. P., Mäkelä, J. M., Hämeri, K., and Kulmala, M.: Urban aerosol
553 number size distributions, Atmos, Chem. Phys., 4, 391–411, https://doi.org/10.5194/acp-4-391-
554 2004, 2004.
555 Hussein, T., Dal Maso, M., Petäjä, T., Koponen, I. K., Paatero, P., Aalto, P. P., Hämeri, K., and Kulmala,
556 M.: Evaluation of an automatic algorithm for fitting the particle number size distributions, Boreal
557 Environ. Res., 10, 337–355, 2005.
558 Jimenez, J. L., Jayne, J. T., Shi, Q., Kolb, C. E., Worsnop, D. R., Yourshaw, I., Morris, J. W.: Ambient

559 aerosol sampling using the aerodyne aerosol mass spectrometer, J. Geophys. Res.-Atmos., 108(D7),
560 https://doi.org/ https://doi.org/10.1029/2001JD001213, 2003.
561 Kim, Y.P., Seinfeld, J.H., Saxena, P.: Atmospheric gas-aerosol equilibrium I. Thermodynamic model,
562 Aerosol Sci. Technol., 19 (2), 157–181, https://doi.org/10.1080/02786829308959628, 1993.
563 Kitamori, Y., Mochida, M., Kawamura, K.: Assessment of the aerosol water content in urban
564 atmospheric particles by the hygroscopic growth measurements in Sapporo, Japan. Atmos. Environ.,
565 43 (21), 3416–3423, https://doi.org/10.1016/j.atmosenv.2009.03.037, 2009.
566 Kuang Y., Zhao C.S., Ma N., Liu H.J., Bian Y.X., Tao J.C. and Hu M.: Deliquescent phenomena of
567 ambient aerosols on the North China Plain, Geophys Res Lett, 43, 8744-8750,
568 https://doi.org/10.1002/2016GL070273, 2016.
569 Kuang, Y., Zhao, C. S., Zhao, G., Tao, J. C., Xu, W., Ma, N., and Bian, Y. X.: A novel method for
570 calculating ambient aerosol liquid water content based on measurements of a humidified
571 nephelometer system, Atmospheric Measurement Techniques, 11(5), 2967-2982,
572 https://doi.org/10.5194/amt-11-2967-2018, 2018.
573 Lathem, T. L., Beyersdorf, A. J., Thornhill, K. L., Winstead, E. L., Cubison, M. J., Hecobian, A.,
574 Jimenez, J. L., Weber, R. J., Anderson, B. E., and Nenes, A.: Analysis of CCN activity of Arctic
575 aerosol and Canadian biomass burning during summer 2008, Atmos. Chem. Phys., 13, 2735–2756,
576 https://doi.org/10.5194/acp-13-2735- 2013, 2013.
577 Liao, H., Seinfeld, J. H.: Global impacts of gas-phase chemistry aerosol interactions on direct radiative
578 forcing by anthropogenic aerosols and ozone, J. Geophys. Res.-Atmos., 110 (D18).
579 https://doi.org/10.1029/ 2005JD005907, 2005.
580 Li, Z., Lau, W. M., Ramanathan, V., Wu, G., Ding, Y., Manoj, M. G., Liu, J., Qian, Y., Li, J., and Zhou,
581 T.: Aerosol and mon- soon climate interactions over Asia, Rev. Geophys., 54, 866–929,
582 https://doi.org/10.1002/2015RG000500, 2016.
583 Liu, S., Hu, M., Wu, Z., Wehner, B., Wiedensohler, A., and Cheng, Y.: Aerosol number size distribution
584 and new particle formation at a rural/coastal site in Pearl River Delta (PRD) of China, Atmos.
585 Environ., 42, 6275–6283, https://doi.org/10.1016/j.atmosenv.2008.01.063, 2008.
586 Mei F., Setyan A., Zhang Q. and Wang J.: CCN activity of organic aerosols observed downwind of
587 urban emissions during CARES, Atmos. Chem. Phys., 13, 12155-12169,
588 https://doi.org/10.5194/acp-13-12155-2013, 2013.
589 Moore, R. H., Bahreini, R., Brock, C. A., Froyd, K. D., Cozic, J., Holloway, J. S., Middlebrook, A. M.,
590 Murphy, D. M., and Nenes, A.: Hygroscopicity and composition of Alaskan Arctic CCN during
591 April 2008, Atmos. Chem. Phys., 11, 11807–11825, https://doi.org/10.5194/acp-11-11807-2011,
592 2011.

Nenes, A., Pandis, S.N., Pilinis, C.: ISORROPIA: a new thermodynamic equilibrium model for multiphase multicomponent inorganic aerosols, Aquat. Geochem., 4 (1), 123–152, https://doi.org/10.1023/A:1009604003981, 1998.

Nguyen, T. K. V., Zhang, Q., Jimenez, J. L., Pike, M., Carlton, A. G.: Liquid Water: Ubiquitous Contributor to Aerosol Mass, Environ. Sci. Technol. Lett., 3 (7), 257−263, https://doi.org/10.1021/acs.estlett.6b00167, 2016.

Paatero, P., & Tapper, U. (2010). Positive matrix factorization: a non-negative factor model with optimal utilization of error estimates of data values. Environmetrics, 5(2), 111-126.

Petters, M. D. and Kreidenweis, S. M.: A single parameter representation of hygroscopic growth and cloud condensation nucleus activity, Atmos. Chem. Phys., 7, 1961–1971, https://doi.org/10.5194/acp-7- 1961-2007, 2007.

Sareen, N., Waxman, E. M., Turpin, B. J., Volkamer, R., Carlton, A. G.: Potential of Aerosol Liquid Water to Facilitate Organic Aerosol Formation: Assessing Knowledge Gaps about Precursors and Partitioning, Environ. Sci. Technol., 51 (6), 3327−3335, https://doi.org/10.1021/acs.est.6b04540, 2017.

Seinfeld, H. J., Pandis, N. S.: Atmospheric Chemistry and Physics: From Air Pollution to Climate Change, Taylor & Francis Group, https://doi.org/10.1080/00139157.1999.10544295, 2006.

Sjogren, S., Gysel, M., Weingartner, E., Baltensperger, U., Cubison, M. J., Coe, H., Zardini, A. A., Marcolli, C., Krieger, U. K., and Peter, T.: Hygroscopic growth and water uptake kinetics of two-phase aerosol particles consisting of ammonium sulfate, adipic and humic acid mixtures, J. Aerosol. Sci., 38, 157–171, https://doi.org/10.1016/j.jaerosci.2006.11.005, 2007.

Song, S., Gao, M., Xu, W., et al.: Possible heterogeneous chemistry of hydroxyl-methane-sulfonate (HMS) in northern China winter haze, Atmos. Chem. Phys., 19(2): 1357-1371, https://doi.org/10.5194/acp-19-1357-2019, 2019.

Stanier, C.O., Khlystov, A.Y., Chan, W.R., Mandiro, M., Pandis, S.N.: A method for the in situ measurement of fine aerosol water content of ambient aerosols: The Dry Ambient Aerosol Size Spectrometer (DAASS), Aerosol Sci. Technol., 38 (1), 215–228, https://doi.org/10.1080/02786820390229525, 2004.

Stokes, R. H. and Robinson, R. A.: Interactions in aqueous nonelectrolyte solutions. I. Solute-solvent equilibria, J. Phys. Chem., 70, 2126–2131, https://doi.org/10.1021/j100879a010, 1966.

Sun, Y., Zhuang, G., Tang, A., Wang, Y., An, Z.: Chemical characteristics of $PM_{2.5}$ and PM_{10} in haze-fog episodes in Beijing, Environ. Sci. Technol., 40, 3148-3155, https://doi.org/10.1021/es051533g, 2006.

626 Sun, Y., Z. F. Wang, P. Q. Fu, T. Yang, Q. Jiang, H. B. Dong, J. Li, and J. J. Jia.: Aerosol composition,
627 sources and processes during wintertime in Beijing, China, Atmos. Chem. Phys., 13(9), 4577–4592,
628 https://doi.org/10.5194/acp-13-4577-2013, 2013.
629 Sun Y., Chen C., Zhang Y., Xu W., Zhou L., Cheng X., Zheng H., Ji D., Jie L. and Xiao T.: Rapid
630 formation and evolution of an extreme haze episode in Northern China during winter 2015, Sci.
631 Rep., 6(1):27151, https://doi.org/10.1038/srep27151, 2016a.
632 Sun, Y., Wang, Z., Wild, O., Xu, W., Chen, C., Fu, P., Du, W., Zhou, L., Zhang, Q., and Han, T.: "APEC
633 Blue": Secondary Aerosol Reductions from Emission Controls in Beijing, Sci. Rep., 6, 20668,
634 https://doi.org/10.1038/srep20668, 2016b.
635 Surratt, J. D., Kroll, J. H., Kleindienst, T. E., Edney, E. O., Claeys, M., Sorooshian, A., Ng, N. L.,
636 Offenberg, J. H., Lewandowski, M., Jaoui, M., Flagan, R. C., Seinfeld, J. H.: Evidence for
637 organosulfates in secondary organic aerosol, Environ. Sci. Technol., 41, 517−527,
638 https://doi.org/10.1021/es062081q, 2007.
639 Swietlicki, E., Zhou, J., Berg, O. H., Martinsson, B. G., Frank, G., Cederfelt, S. I., Dusek, U., Berner,
640 A., Birmili, W., Wiedensohler, A., Yuskiewicz, B., and Bower, K. N.: A closure study of sub-
641 micrometer aerosol particle hygroscopic behaviour, Atmos. Res., 50, 205–240,
642 https://doi.org/10.1016/S0169-8095(98)00105-7, 1999.
643 Tan, H., Cai, M., Fan, Q., Liu, L., Li, F., & Chan, P. W., et al.: An analysis of aerosol liquid water
644 content and related impact factors in pearl river delta, Science of The Total Environment, 579, 1822-
645 1830, https://doi.org/10.1016/j.scitotenv.2016.11.167, 2017.
646 Tao, W. K., Chen, J. P., Li, Z., Wang, C., and Zhang, C.: Impact of Aerosols on Convective Clouds and
647 Precipitation, Rev. Geo. phys., 50, 1–62, https://doi.org/10.1029/2011RG000369, 2012.
648 Thornton, J. A., Braban, C. F., Abbatt, J. P. D.: N_2O_5 hydrolysis on sub-micron organic aerosols: the
649 effect of relative humidity, particle phase, and particle size. Atmos. Chem. Phys., 5 (20), 4593−4603,
650 https://doi.org/10.1039/b307498f, 2003.
651 Topping D O, Mcfiggans G B, Coe H.: A curved multi-component aerosol hygroscopicity model
652 framework: Part 1 – Inorganic compounds, Atmos. Chem. Phys., 5(5): 1205-1222,
653 https://doi.org/10.5194/acp-5-1205-2005, 2005.
654 Wahner, A., Mentel, T. F., Sohn, M., Stier, J.: Heterogeneous reaction of N_2O_5 on sodium nitrate
655 aerosol, J. Geophys. Res. Atmos, 103 (D23), 31103−31112, https://doi.org/10.1029/1998JD100022,
656 1998.
657 Wang, G., Zhang, R., Gomez, M. E., Yang, L., Levy Zamora, M., Hu, M., Lin, Y., Peng, J., Guo, S.,
658 Meng, J., Li, J., Cheng, C., Hu, T., Ren, Y., Wang, Y., Gao, J., Cao, J., An, Z., Zhou, W., Li, G.,
659 Wang, J., Tian, P., MarreroOrtiz, W., Secrest, J., Du, Z., Zheng, J., Shang, D., Zeng, L., Shao, M.,

Wang, W., Huang, Y., Wang, Y., Zhu, Y., Li, Y., Hu, J., Pan, B., Cai, L., Cheng, Y., Ji, Y., Zhang, F., Rosenfeld, D., Liss, P. S., Duce, R. A., Kolb, C. E., Molina, M. J.: Persistent sulfate formation from London Fog to Chinese haze, Proc. Natl. Acad. Sci. U. S. A., 113 (48), 13630−13635, https://doi.org/10.1073/pnas.1616540113, 2016.

Wang, H., Lu, K., Chen, X., Zhu, Q., Chen, Q., Guo, S., Jiang, M., Li, X., Shang, D., Tan, Z., Wu, Y., Wu, Z., Zou, Q., Zheng, Y., Zeng, L., Zhu, T., Hu, M., Zhang, Y.: High N_2O_5 Concentrations Observed in Urban Beijing: Implications of a Large Nitrate Formation Pathway, Environ. Sci. Technol. Lett., 4 (10), 416−420, https://doi.org/10.1021/acs.estlett.7b00341, 2017.

Wang, T., Nie, W., Gao, J., Xue, L. K., Gao, X. M., Wang, X. F., Qiu, J., Poon, C. N., Meinardi, S., Blake, D., Wang, S. L., Ding, A. J., Chai, F. H., Zhang, Q. Z., and Wang, W. X.: Air quality during the 2008 Beijing Olympics: secondary pollutants and regional impact, Atmos. Chem. Phys., 10, 7603–7615, https://doi.org/10.5194/acp-10-7603-2010, 2010.

Wang, Y., Zhang, Q., Jiang, J., Zhou, W., Wang, B., He, K., Duan, F., Zhang, Q., Philip, S., and Xie, Y.: Enhanced sulfate formation during China's severe winter haze episode in January 2013 missing from current models, J. Geophys. Res.-Atmos., 119, 10425– 10440, https://doi.org/10.1002/2013JD021426, 2014.

Wang Y., Zhang F., Li Z., Tan H., Xu H., Ren J., Zhao J., Du W. and Sun Y.: Enhanced hydrophobicity and volatility of submicron aerosols under severe emission control conditions in Beijing, Atmos Chem Phys, 17, 5239-5251, https://doi.org/10.5194/acp-17-5239-2017, 2017.

Wang Y., Li Z., Zhang Y., Du W., Zhang F., Tan H., Xu H., Fan T., Jin X., Fan X., Dong Z., Wang Q. and Sun Y.: Characterization of aerosol hygroscopicity, mixing state, and CCN activity at a suburban site in the central North China Plain, Atmos. Chem. Phys., 18, 11739-11752, https://doi.org/10.5194/acp-18-11739-2018, 2018.

Wehner, B., Birmili, W., Ditas, F., Wu, Z., Hu, M., Liu, X., Mao, J., Sugimoto, N., and Wiedensohler, A.: Relationships between sub micrometer particulate air pollution and air mass history in Beijing, China, 2004–2006, Atmos. Chem. Phys., 8, 6155–6168, https://doi.org/10.5194/acp-8-6155-2008, 2008.

Wexler, A.S., Clegg, S.L.: Atmospheric aerosol models for systems including the ions H^+, NH_4^+, Na^+, SO_4^{2-}, NO_3^-, Cl^-, Br^-, and H_2O, J. Geophys. Res.-Atmos., 107 (D14): 14-14, https://doi.org/10.1029/2001JD000451, 2002.

Whitby, K. T.: The physical characteristics of sulfur aerosols, Atmos. Environ., 12, 135–159, https://doi.org/10.1016/j.atmosenv.2007.10.057, 1978.

Wiedensohler A.: An approximation of the bipolar charge distribution for particles in the submicron size range, J. Aerosol Sci., 19, 387–389, https://doi.org/10.1016/0021-8502(88)90278-9, 1988.

694 Wu, G. X., Li, Z. Q., Fu, C. B., Zhang, X. Y., Zhang, R. Y., Zhang, R. H., Zhou, T. J., Li, J. P., Li, J.
695 D., and Zhou, D. G.: Advances in studying interactions between aerosols and monsoon in China,
696 Science China Earth Science, 59, 1–16, https://doi.org/10.1007/s11430-015-5198-z, 2016.
697 Wu, Z., Wang, Y., Tan, T., Zhu, Y., Li, M., & Shang, D., et al.: Aerosol liquid water driven by
698 anthropogenic inorganic salts: implying its key role in the haze formation over north china
699 plain, Environ. Sci. Technol. Lett., 5(3), 160-166, https://doi.org/10.1021/acs.estlett.8b00021, 2018.
700 Xu, L., Guo, H., Boyd, C. M., Klein, M., Bougiatioti, A., Cerully, K. M., Hite, J. R., Isaacman-
701 VanWertz, G., Kreisberg, N. M., Knote, C., Olson, K., Koss, A., Goldstein, A. H., Hering, S. V., de
702 Gouw, J., Baumann, K., Lee, S.-H., Nenes, A., Weber, R. J., and Ng, N. L.: Effects of anthropogenic
703 emissions on aerosol formation fromisoprene and monoterpenes in the southeastern United States,
704 P. Natl. Acad. Sci., 112, 37–42, https://doi.org/10.1073/pnas.1417609112, 2015.
705 Xu, W., Han, T., Du, W., Wang, Q., Chen, C., Zhao, J., Zhang, Y., Li, J., Fu, P., Wang, Z., Worsnop, D.
706 R., Sun, Y.: Effects of Aqueous- Phase and Photochemical Processing on Secondary Organic
707 Aerosol Formation and Evolution in Beijing, China, Environ. Sci. Technol. Lett., 51 (2), 762−770,
708 https://doi.org/10.1021/acs.est.6b04498, 2017.
709 Zheng, B., Zhang, Q., Zhang, Y., He, K. B., Wang, K., Zheng, G. J., Duan, F. K., Ma, Y. L., Kimoto,
710 T.: Heterogeneous chemistry: a mechanism missing in current models to explain secondary
711 inorganic aerosol formation during the January 2013 haze episode in North China, Atmos. Chem.
712 Phys., 15 (4), 2031−2049, https://doi.org/10.5194/acp-15-2031-2015, 2015.
713 Zieger, P., Väisänen, O., Corbin, J. C., Partridge, D. G., Bastelberger, S., Mousavi-Fard, M., Rosati,
714 B., Gysel, M., Krieger, U. K., Leck, C., Nenes, A., Riipinen, I., Virtanen, A., and Salter, M. E.:
715 Revising the hygroscopicity of inorganic sea salt particles, Nature communications, 8, 15883,
716 https://doi.org/10.1038/ncomms15883, 2017.
717
718

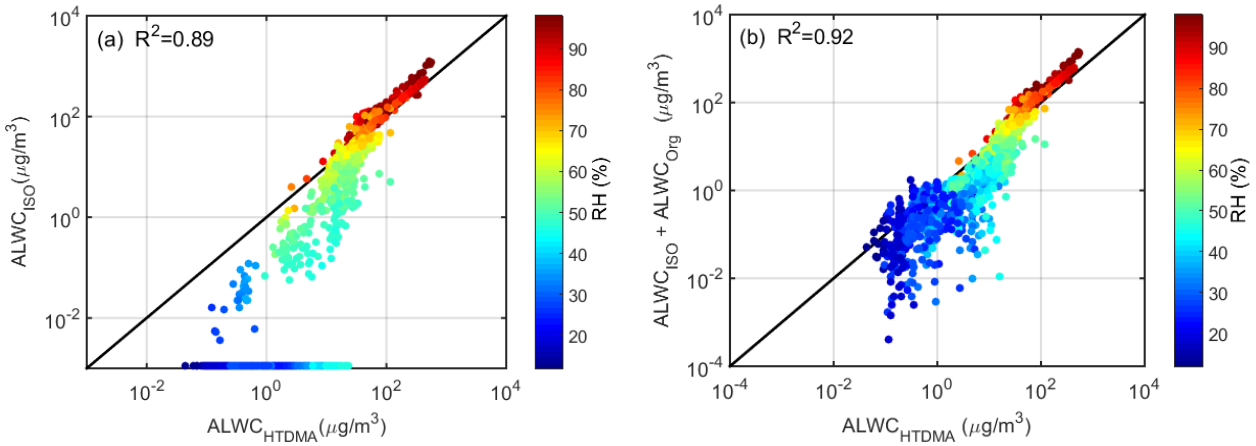

719

Figure 1. Comparison between $ALWC_{HTDMA}$ and (a) $ALWC_{ISO}$ and (b) the sum of $ALWC_{ISO}$ and $ALWC_{Org}$. $ALWC_{HTDMA}$ refers to calculated ALWC based on the measured growth factor and PNSDs, $ALWC_{ISO}$ refers to simulated ALWC from the ISORROPIA II model, and $ALWC_{Org}$ refers to the inferred ALWC contributed by organic species. The coefficient of determination R^2 is given in each panel. The color of the dots denotes the ambient RH; the solid line denotes the 1:1 line.

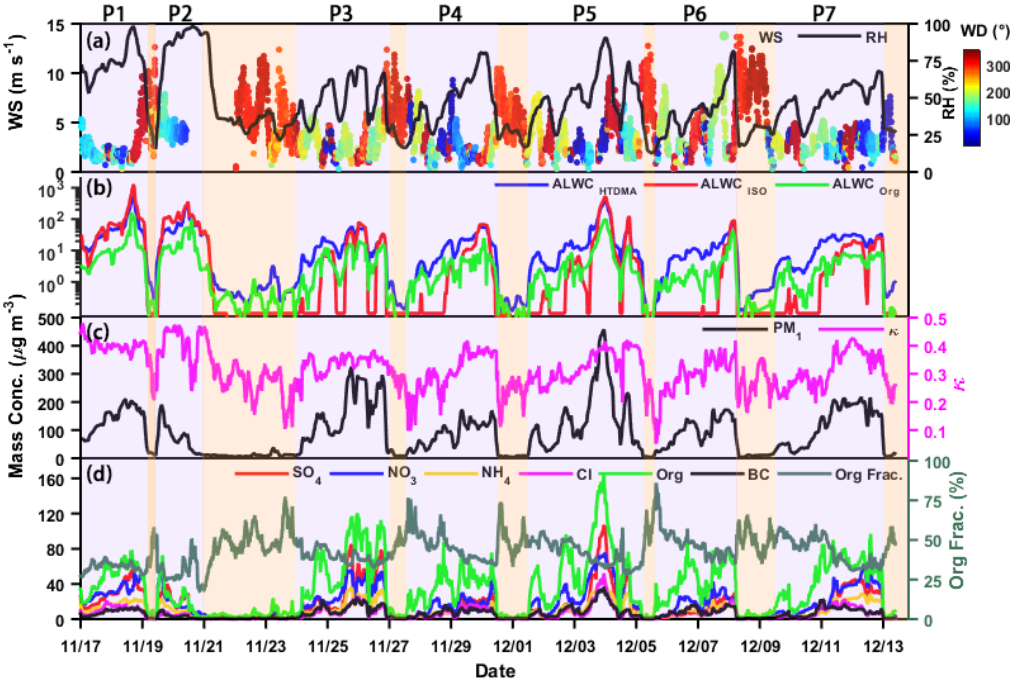

Figure 2. Time series of (a) wind speed (WS, left y-axis), ambient relative humidity (RH, right y-axis), and wind direction (WD, colored dots), (b) $ALWC_{HTDMA}$ (in blue), $ALWC_{ISO}$ (in red), and $ALWC_{Org}$ (in green), (c) PM_1 mass concentration (left y-axis) and hygroscopicity parameter (κ, right y-axis) calculated using the ZSR model described by Eq. (7), and (d) mass concentrations of aerosol species in PM_1 (left y-axis) and organic aerosol mass fraction (right y-axis). Seven polluted episodes (segments of the time series with a purple background) are selected for examination.

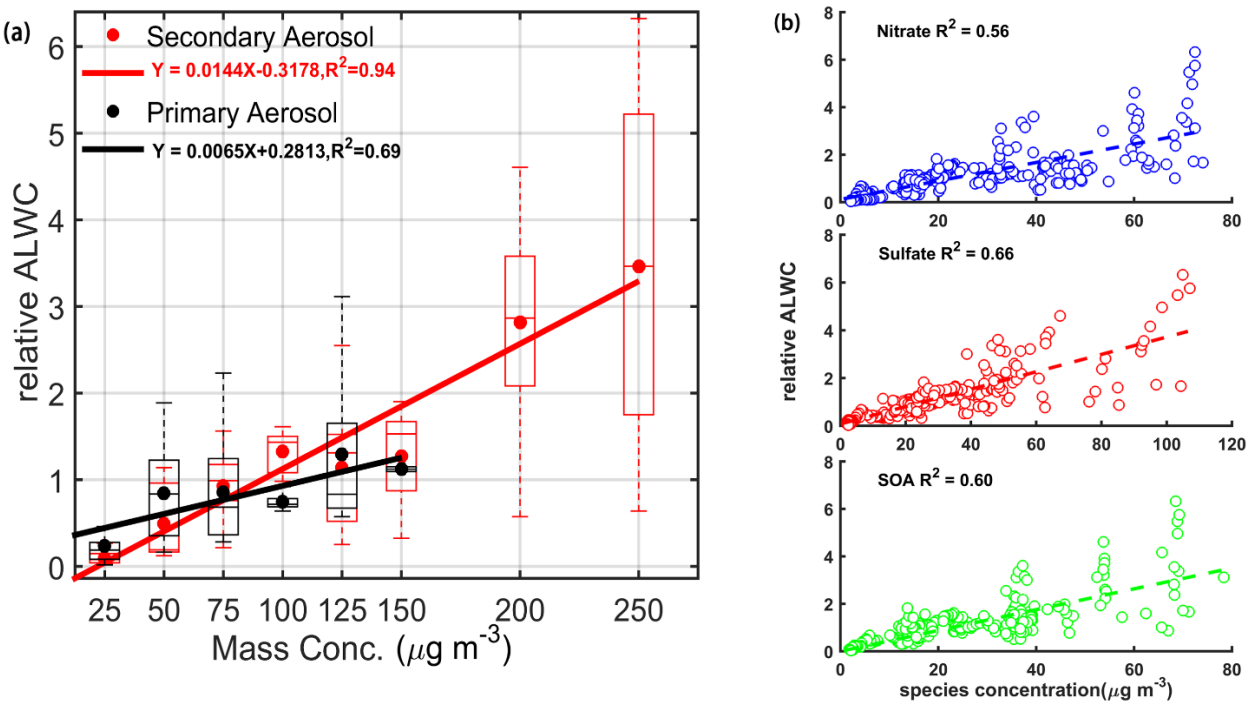

734

735 **Figure 3. The correlation analysis between relative ALWC and (a) primary (in black) and secondary (in red) aerosol**
736 **mass concentrations, and (b) nitrate, sulfate, and secondary organic aerosol (SOA) mass concentrations. Panel (a)**
737 **shows mean relative ALWCs (solid dots) with boxes showing the 25th, 50th, and 75th percentiles. The extremities**
738 **show the 5th and 95th percentiles. The solid lines in (a) and the dashed lines in (b) both represent the corresponding**
739 **best-fit lines from linear regression.**

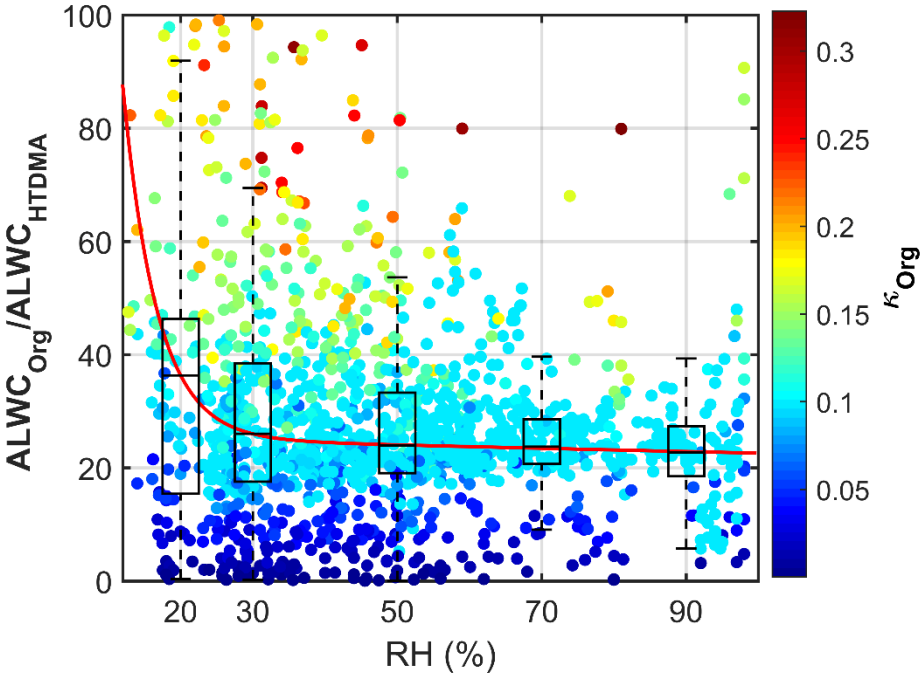

740

741 **Figure 4. The variation of the fraction of $ALWC_{Org}$ in total ALWC ($ALWC_{HTDMA}$) with the ambient relative humidity**
742 **(RH). The color of the dots denotes the hygroscopicity parameter of organics (κ_{Org}). The boxes show the fraction of**

743 **$ALWC_{Org}$ with the 25th, 50th, and 75th percentiles. The extremities show the 5th and 95th percentiles. The red line**

744 **shows the fitting curve with the function $y = ae^{bx}$.**

745

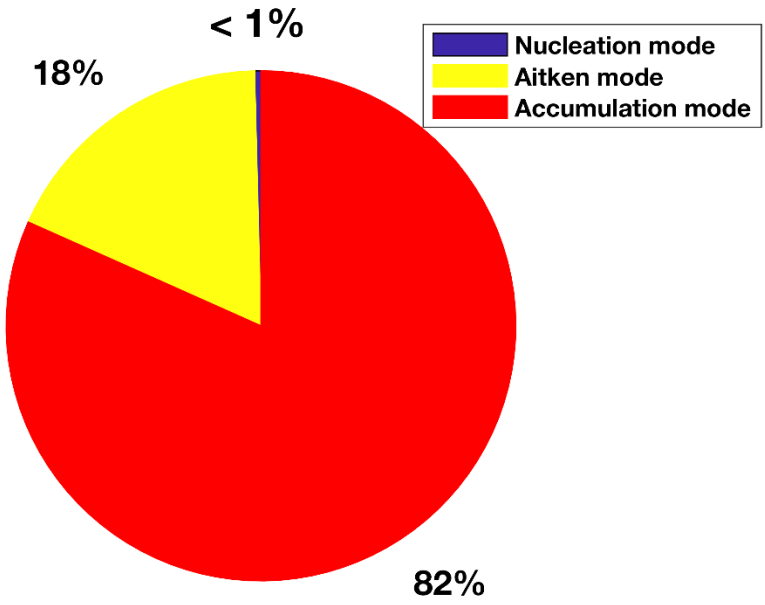

746

747 **Figure 5. The contribution of particles different modes to $ALWC_{HTDMA}$**

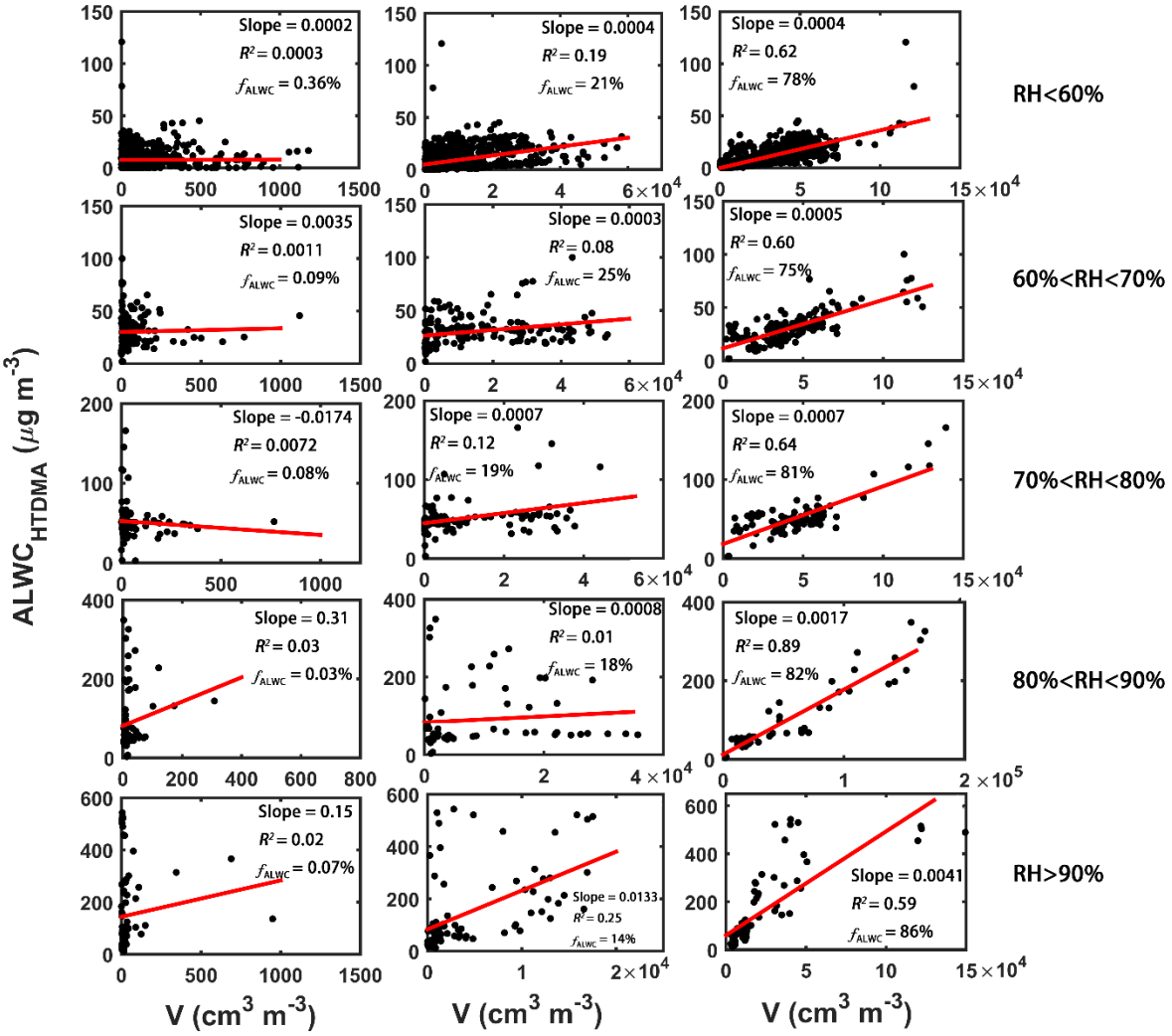

Figure 6. The correlation analysis between $ALWC_{HTDMA}$ and the volume concentration of nucleation mode (left column), Aitken mode (middle column), and accumulation mode (right column) particles under different ambient relative humidity (RH) conditions. The average contribution of each mode particles to ALWC under different ambient RH conditions is denoted by f_{ALWC}. The red lines represent the best-fit lines from linear regression.

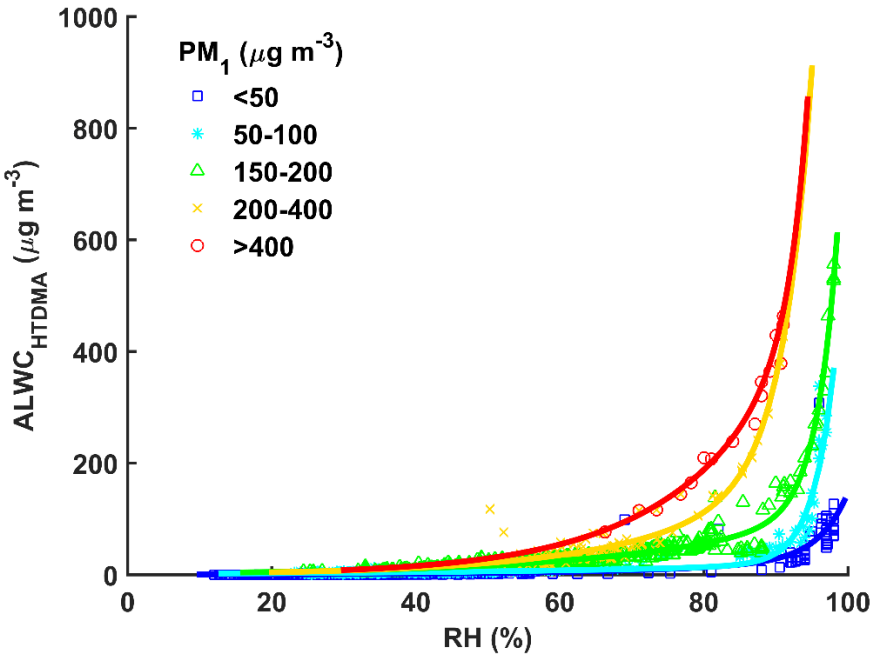

754

755 **Figure 7. The dots show how $ALWC_{HTDMA}$ varies with the ambient relative humidity (RH) for different PM_1 mass**

756 **concentration ranges (colored symbols). The colored curves represent the best-fit lines through the data using the**

757 **fitting function $y = ae^{bx}$.**

758

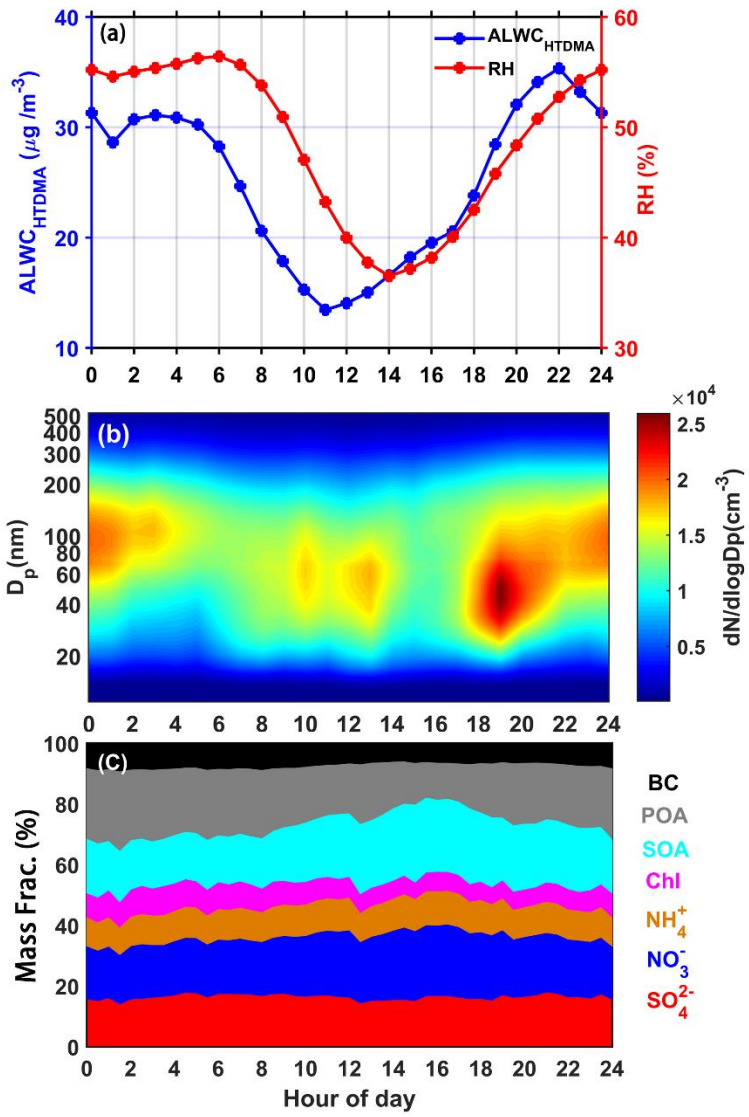

759

760 **Figure 8. Diurnal variations of (a) ALWC$_{HTDMA}$ (in blue) and ambient RH (in red), (b) particle number size**

761 **distribution, and (c) the mass fraction of different chemical species. The time is in Beijing time.**

762

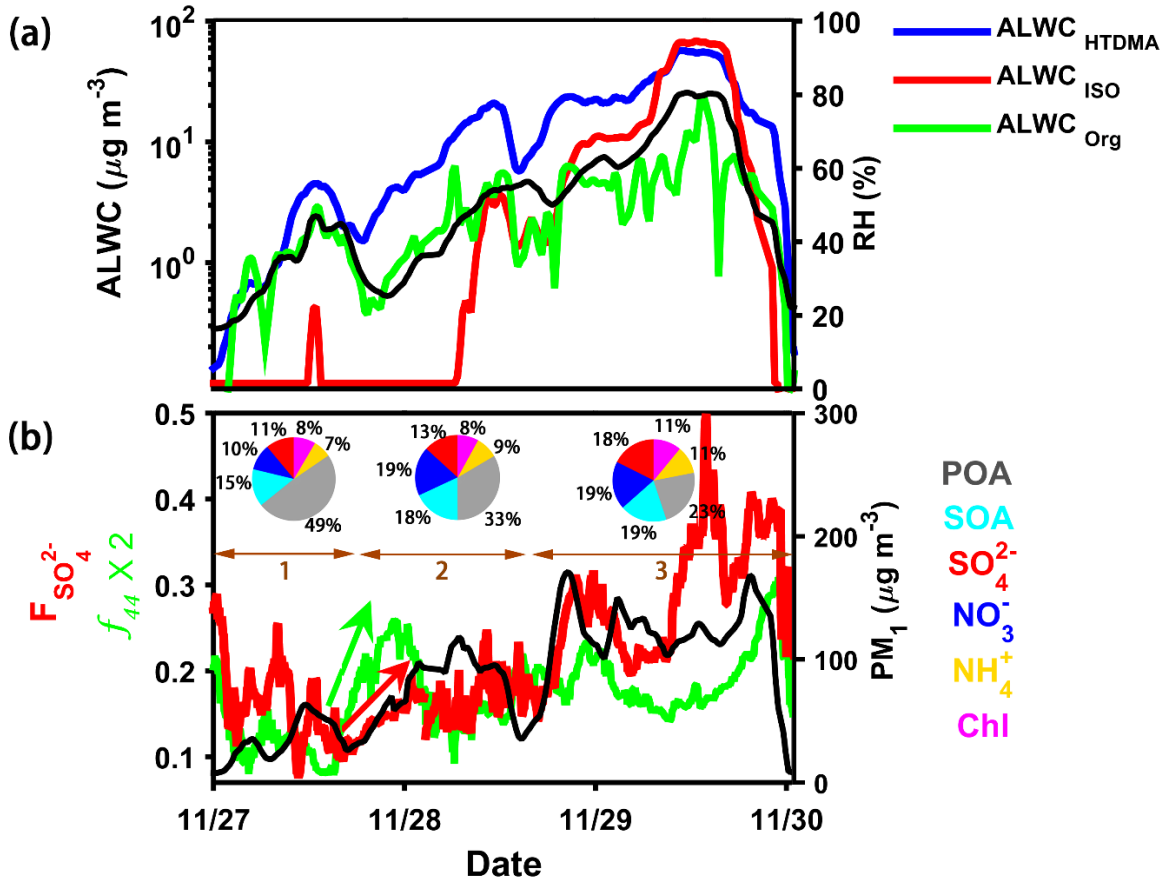

763

764 **Figure 9. Time series of (a) ALWC$_{HTDMA}$ (in blue), ALWC$_{ISO}$ (in red), ALWC$_{Org}$ (in green), and RH (right y-axis), and**

765 **(b) the sulfur oxidation ratio (F_{SO4}^{2-}), f_{44}, and PM$_1$ mass concentration (right y-axis) during the P4 case in Figure 2.**

766 **The pie charts in (b) represent the average chemical compositions of PM$_1$ during three stages of the pollution event**

767 **(denoted by brown horizontal lines). The red and green arrows in (b) indicate the rapid increase in F_{SO4}^{2-} and f_{44} at**

768 **the initial stage.**

769